Ultrafast photochemistry of methyl hydroperoxide on ice particles

M. A. Kamboures[a], S. A. Nizkorodov[a], and R. B. Gerber[a,b,1]

[a]Department of Chemistry, University of California, Irvine, CA 92697-2025; and [b]Institute of Chemistry and Fritz Haber Center, Hebrew University, Jerusalem 91904, Israel

Edited by Barbara J. Finlayson-Pitts, University of California, Irvine, CA, and approved September 17, 2009 (received for review July 15, 2009)

Simulations show that photodissociation of methyl hydroperoxide, CH_3OOH, on water clusters produces a surprisingly wide range of products on a subpicosecond time scale, pointing to the possibility of complex photodegradation pathways for organic peroxides on aerosols and water droplets. Dynamics are computed at several excitation energies at 50 K using a semiempirical PM3 potential surface. CH_3OOH is found to prefer the exterior of the cluster, with the CH_3O group sticking out and the OH group immersed within the cluster. At atmospherically relevant photodissociation wavelengths the OH and CH_3O photofragments remain at the surface of the cluster or embedded within it. However, none of the 25 completed trajectories carried out at the atmospherically relevant photodissociation energies led to recombination of OH and CH_3O to form CH_3OOH. Within the limited statistics of the available trajectories the predicted yield for the recombination is zero. Instead, various reactions involving the initial fragments and water promptly form a wide range of stable molecular products such as CH_2O, H_2O, H_2, CO, CH_3OH, and H_2O_2.

air–water interface | molecular dynamics | peroxides | photodissociation

Photoinduced processes at surfaces of water or ice are of interest in atmospheric chemistry and other areas. However, molecular-level understanding of such processes is largely lacking, because the systems and the interactions involved are complex. In this article, we explore, as a fundamental prototype, the photodissociation of the simplest organoperoxide, CH_3OOH, on an ice particle. A major motivation for studying this peroxide is its relevance to atmospheric chemistry, as discussed in refs. 1–11 and references therein. Methyl hydroperoxide is typically present in cloud water droplets in micromolar concentrations (7, 12, 13) and is also likely to occur in aerosols (4, 14). The fate of CH_3OOH in water droplets may influence its role as a reservoir for HO_x because this peroxide is known to be a major source of OH at high tropospheric altitudes (10, 15). Fenton-like reactions involving CH_3OOH and Fe(II) serve as an important source of aqueous HO_2 radicals (16). Finally, recent evidence suggests that reactions between peroxides and isoprene oxidation products lead to the formation of tetrols, thus contributing to the production of secondary organic aerosols (17).

It is well established that gas-phase CH_3OOH photolyzes under UV-visible excitation to form CH_3O and OH with a quantum yield approaching unity (8, 18–23). Because of the moderate solubility of CH_3OOH, it is also likely to undergo condensed-phase photolysis after being taken up by aqueous particles and ice particles and contribute to the production of aqueous free radicals (24). To the best of our knowledge, only two prior experiments examined photolysis of CH_3OOH in liquid water (9) and ice particles.[†] Each of these studies identified CH_2O and H_2O as major products, suggesting that the photochemistry of CH_3OOH is considerably more complicated in condensed-phase environments. Unlike the gas-phase photolysis of CH_3OOH (5, 8), its condensed-phase photolysis has not been investigated by theoretical methods. We have used a theoretical study to trace the dynamics of the primary photolysis products, CH_3O and OH, on a small water cluster with atomistic simulations.

There are many precedents of using molecular dynamics-based approaches for investigating photochemistry in condensed environments (26–31) and using small water clusters as representative model systems of aqueous reactivity (32, 33). For example, photolysis of water in crystalline ice was examined by using force fields to approximate the potentials (26). Photodissociation of HCl adsorbed on ice was studied with an approach in which the hydrogen fragment was described quantum-mechanically and the chlorine fragment and the water molecules were treated classically (27, 28). A similar quantum mechanics/molecular mechanics strategy was used to investigate the photodissociation of chlorine peroxide on ice (29). Several investigators have resorted to freezing certain degrees of freedom during their simulations (30, 31). This work uses PM3 electronic structure method (34) for the "on-the-fly" generation of the forces along the atomic trajectories (35), permitting efficient simulation for relatively large clusters. Present calculations do not involve freezing selected coordinates or reducing interactions to force fields that may artificially prevent unanticipated chemical processes. Our results show that even for a relatively small polyatomic molecule, such as CH_3OOH, photolysis on ice produces a large variety of chemical outcomes. It is anticipated that for larger organic peroxides the variety of competing chemical pathways will be even greater. The capability of the method we have used to describe diverse, perhaps unexpected, chemical reactions is essential for simulating the photochemistry of organic peroxides in water. We anticipate that this method can also be used to simulate other photochemical processes occurring on or within water or other condensed environments.

Results

The CH_3OOH molecule was positioned at the surface of a cluster of 20 water molecules, and a dynamics simulation was ran at 50 K under the influence of the PM3 potential. The trajectory was propagated for 30 ps. Twenty randomly chosen configurations, between 10 and 29 ps, were analyzed. Fig. 1 displays a representative snapshot of the cluster. In this and all other snapshots CH_3OOH remained on the surface of the cluster. In simulations that intentionally positioned CH_3OOH in the middle of the cluster, CH_3OOH migrated toward the surface. The CH_3O carbon and oxygen atoms were equidistant, on average, from the center of mass of the cluster (2.9 ± 0.2 and 2.9 ± 0.1 Å, respectively). In contrast, the OH oxygen atom was found closer to the center of the cluster, 1.8 ± 0.2 Å, and the OH hydrogen was typically found at an intermediate location, 2.6 ± 0.2 Å. Fig. 1

Author contributions: M.A.K., S.A.N., and R.B.G. designed research; M.A.K. performed research; M.A.K. analyzed data; and M.A.K., S.A.N., and R.B.G. wrote the paper.

The authors declare no conflict of interest.

This article is a PNAS Direct Submission.

[1]To whom correspondence should be addressed. E-mail: bgerber@uci.edu.

†Schrems O, Gand M, Ignatov SK, Sennikov PG, Poster presentation, Seventh International Conference on Low-Temperature Chemistry, August 24–29, 2008, Helsinki, Finland.

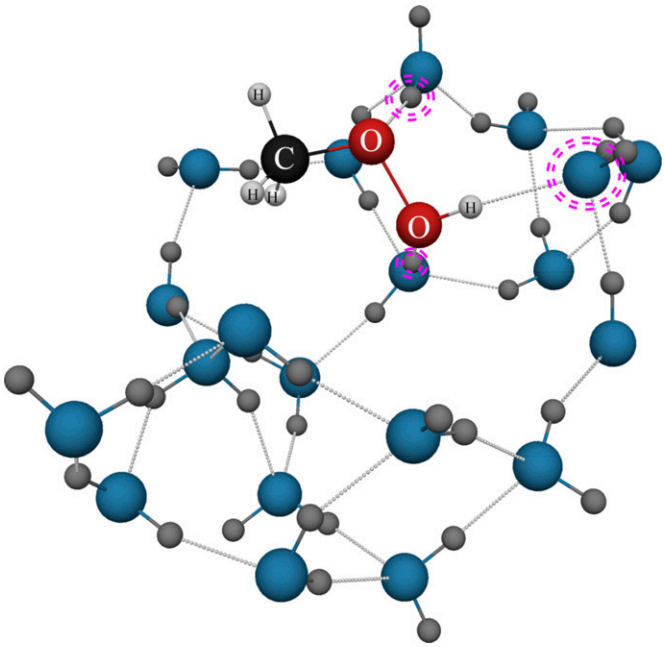

Fig. 1. A representative structure of CH_3OOH on a 20-molecule H_2O ice cluster at 50 K. Pink halos indicate water atoms that are hydrogen-bonded to CH_3OOH.

shows a typical bonding pattern, with the two oxygen atoms and peroxidic hydrogen atom in CH_3OOH forming hydrogen bonds with neighboring water molecules. This pattern was observed for all 20 sampled configurations.

A total of 120 photolysis simulations were performed. Each of these simulations was constructed from 1 of 20 unique starting geometries and six different photon energies. The vertical transitions corresponding to the six photon energies are depicted in Fig. 2. The 6.7-eV transition corresponds to a Franck–Condon excitation from the lowest energy state. The transition at 8.4 eV corresponds to a higher-energy UV photoexcitation. The 4.8-, 4.1-, and 2.9-eV transitions correspond to the atmospherically relevant photoexcitation energies in the near-UV and visible regions of the solar spectrum.

Table 1 presents key results for these photolysis simulations, sorted by the photon energy, including the fraction of successfully completed trajectories, probabilities of recombination and caging for each of the photolysis fragment, and the final cluster size.

The recombination reaction

$$CH_3O + OH \rightarrow CH_3OOH$$

occurred only 25% of the time for the 0.39-eV excitation even though the fragments were assigned only random thermal velocities at the beginning of this simulation (no recoil fragment from photolysis). In each of these cases the simulations showed that the fragments approached one another in an oscillating fashion. The amplitude of oscillation tended to decrease over time until the peroxide bond distance was relatively constant. Recombination never occurred at the atmospherically relevant excitation energies in which the fragments were forced to recoil from each other after the O—O bond cleavage. In a few instances, the fragments did approach one another, in the cluster, after a higher energy photolysis. These encounters, however, tended to stimulate ejection of H or H_2 from the CH_3O fragment rather than lead to recombination. This finding indicates that, despite the anticipated molecular cage effects, recombination is very unlikely for a photolyzed CH_3OOH molecule sitting on top of an ice or water surface.

Trajectories resulting in the ejection of CH_3O and/or OH from the cluster were also surprisingly rare, except during the highest energy photolysis events. CH_3O was ejected from the cluster more often than OH because of the initial orientation of CH_3O—OH. In general, r(O—O) was approximately perpendicular to the surface of the water cluster, at the beginning of these simulations, and the

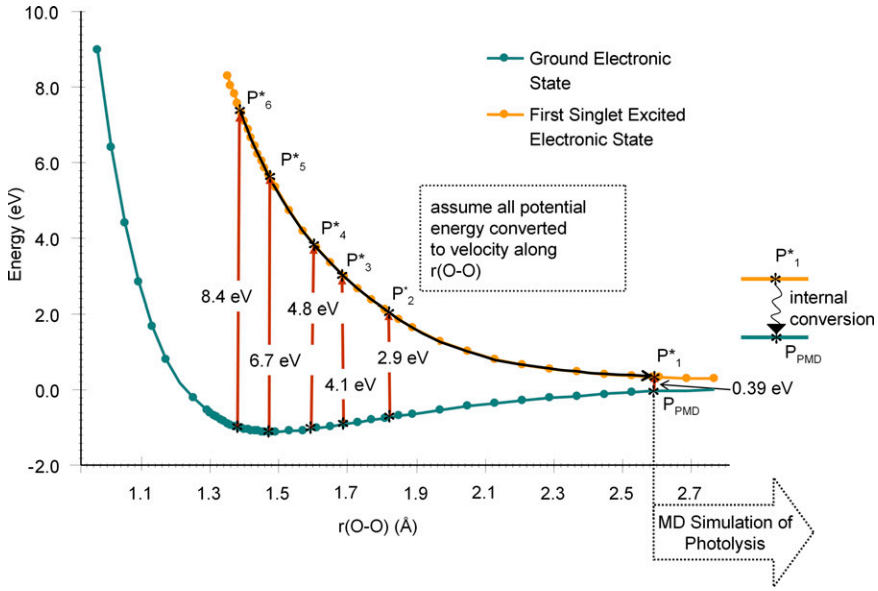

Fig. 2. Ground-state and first excited-state potential energies of CH_3OOH along r(O—O). The lengths of the vertical arrows indicate the photoexcitation energies explored. In each photolysis simulation the system was excited to a point P^*_i. The molecule then dissociated along the excited-state potential, and the decrease in energy along the potential curve r(O—O) was assumed to be entirely converted into the kinetic energy in the r(O—O) coordinate. At P^*_1 it was assumed that the system internally converted to the ground state at P_{PMD} when the simulation commenced. In the actual calculations, the PM3 potential was used rather than the configuration interaction singles (CIS) potential.

Table 1. Data for the photolysis simulations

Photon energy, eV	λ, nm	Simulation completion frequency	Recombination, %	CH_3O escape, %	OH escape, %	Final cluster size, $\mu(\#H_2O) \pm \sigma$
0.39	3,180	20/20	25	0	0	15.9 ± 4.2
2.9	428	7/20	0	0	0	12.3 ± 5.7
4.1	300	8/20	0	18	18	10.9 ± 6.9
4.8	256	10/20	0	0	0	10.1 ± 6.4
6.7	185	17/20	0	88	41	18.1 ± 3.3
8.4	147	16/20	0	100	100	19.2 ± 1.1

Data for the photolysis simulations including the photon energy and wavelength, and the r(O—O) coordinate corresponding to vertical transitions at this energy. The simulation completion frequencies represent the fraction of the 20 trajectories that ran until a point at which the final chemical products and cluster size could be determined. The recombination percentages represent the fraction of the successful trajectories that lead to reformation of CH_3OOH. The escape percentages represent the fraction of trajectories that lead to unreacted escape of CH_3O or OH. The end cluster sizes represent the average size of the largest water cluster after the simulations had ran to completion.

CH_3O group was on the surface. In the ejection events, the OH fragment rapidly recoiled, directly through the center of the cluster, and then exited the opposing surface often colliding with and simultaneously coejecting one to three water molecules. The CH_3O fragment, in contrast, traveled directly away from the surface of the cluster, in a slow, perpendicular manner and was not generally obstructed by neighboring H_2O molecules.

The most exciting result of these simulations was the observation of rich chemistry involving the initial photolysis fragments, with some of the products appearing as early as 0.2 ps. Fig. 3 shows the distribution of chemical products in the 50-K photolysis simulations of CH_3OOH on 20 water molecules. The bars indicate the percentage of the completed simulations that led to a particular chemical species as a final product. Products like CHO, H, O, and $CH_2(OH)_2$, which appeared in only one or two simulations, were not included in Fig. 3. At the three lowest photon energies CH_2O and H_2O were the major products. For example, CH_2O and H_2O formation occurred in 50% of the 4.1-eV simulations, while H_2, CO, CH_3OH, and H_2O_2 formed in the remaining cases. The formation of CH_2O and H_2O took place, in some instances, by the direct abstraction of an H atom from CH_3O by OH. However, a more common pathway was unimolecular dissociation of CH_3O via a CH_2OH intermediate into CH_2O and H, followed by a series of H atom transfers between several water molecules, until an H atom was passed to OH to form H_2O.

Evaporation of water molecules from the cluster was observed in many trajectories. The extent of evaporation can be judged for the final cluster size (Table 1). In general, larger final cluster sizes, i.e., those having a smaller degree of evaporation, were observed for the highest and lowest excitation energies. At the medium, more atmospherically relevant, excitation energies the fragments remained in the cluster after photoexcitation, but tended to release kinetic energy through collisions with water molecules. Additional kinetic energy was released in subsequent chemical reactions. Combined, these effects tended to break apart the clusters, producing the lower final cluster sizes that were observed.

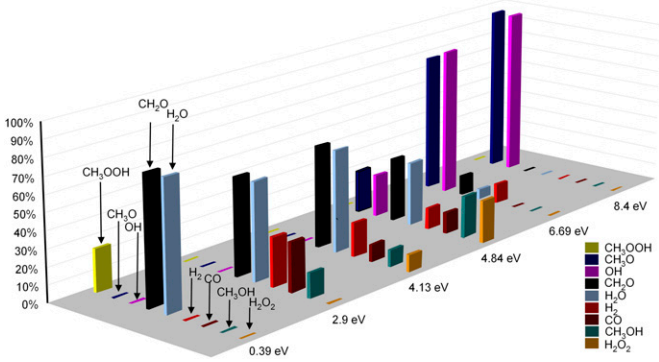

Fig. 3. Chemical product distribution in the photolysis of CH_3OOH on a 50-K ice cluster.

Discussion

We have used a fast method suitable for studying the photochemistry of polyatomic molecules in condensed and/or heterogeneous environments such as atmospheric surfaces. Our calculations indicate that photolysis of CH_3OOH, on the surface of a small water cluster, leads to several wavelength-dependent chemical outcomes, including formation of CH_2O and H_2O, fragment escape, recombination, and formation of other chemical products. Fifty percent of the photolysis simulations at λ = 300 nm (4.1 eV) resulted in the formation of CH_2O and H_2O. Although CH_3O and OH are the major products of CH_3OOH gas-phase photolysis (8, 18–22), the formation of CH_2O and H_2O is thermodynamically favored ($\Delta E = -55$ kcal·mol^{-1}). However, this process is inhibited by an energy barrier that is ≈3.4 kcal·mol^{-1} greater than the energy requirement for the formation of CH_3O and OH in a direct O—O bond cleavage (8). Our simulations show that the surrounding water molecules favor the formation of the lower energy reaction products CH_2O and H_2O.

Monod et al. (9) recently reported the results of experimental studies aimed at characterizing the photolysis of CH_3OOH and the related peroxide C_2H_5OOH under simulated cloud droplet conditions. Millimolar concentrations of the peroxide molecules, dissolved in water, were photolyzed at neutral to acidic pH values at 279 K. In agreement with our simulations they found that, for the photolysis of CH_3OOH at pH 7, the dominant product was CH_2O followed by H_2O_2. Monod et al. (9, 16) have suggested that the CH_3O radical, in water, may quickly isomerize to form CH_2OH. In the simulations we carried out that led to the formation of CH_2O, CH_3O did, in fact, isomerize to CH_2OH. Isomerization to CH_2OH was then followed by the ejection of H and the formation of CH_2O. Finally, it should also be noted that, in a recent investigation, Schrems et al.[†] demonstrated that the photolysis of CH_3OOH in ice generates CH_2O as the major product.

A comparison between CH_3OOH and H_2O_2 is of interest. Gas-phase H_2O_2 promptly breaks into two OH radicals upon UV photoexcitation with nearly 100% efficiency (36). Approximately 50% of the OH+OH pairs formed by photolysis of H_2O_2 in water (37, 38) or ice (39) recombine back into H_2O_2. On the contrary, both experimental and theoretical evidence suggest that recombination is not as efficient in the photolysis of CH_3OOH. Monod et al. (9, 40) attribute this result to the ease

of isomerization of CH_3O radical into CH_2OH radical under aqueous conditions. Our simulations appear to suggest an H-atom transfer from $CH_3O\cdot$ to $\cdot OH$ as a plausible mechanism for the suppression of recombination. Regardless of the interpretation, it is clear that the photolysis product distribution is strongly affected by prompt secondary reactions occurring after the initial O—O bond breaking.

The PM3 method is, in general, not quantitatively accurate. However, for organic molecules at water clusters, the system targeted here, it offers a reasonable balance between efficiency and accuracy. To test the accuracy of this method, we calculated the PM3 electronic binding energy for the H_2O—H_2O dimer and found it to be -3.2 kcal·mol^{-1}. This finding is in good agreement with the existing literature that estimates the true binding energy to be ≈3–5 kcal·mol^{-1} (41–43). Crucial for the applicability of the method is that, after a short time, the propagation could be assumed to take place in the ground electronic state. This assumption certainly neglects reactions that could potentially occur on the electronically excited potential energy surface (PES). In the case of the UV photolysis of organic peroxides, the excited-state chemistry is not likely to make a significant contribution because the initial O—O bond breaking occurs on a femtosecond time scale on a fully repulsive PES (Fig. 2). The semiquantitative agreement with experiment suggests that the dynamics of photodissociation of CH_3OOH in water are governed by the ground-state PES. This approach may therefore be applicable to a broad range of direct photodissociation processes at water and ice surfaces.

Materials and Methods

Molecular dynamics simulations were used to describe the system at thermal equilibrium, before absorption of a photon. An efficient, yet sufficiently realistic, force field is essential for the dynamics simulations. We chose the semiempirical PM3 potential (34) and used it in on-the-fly simulations of the dynamics (35) at 50 K. For a recent review of dynamics simulations of atmospherically relevant processes, including simulations of reactions in water clusters and PM3 for dynamics, refer to ref. 33. The trajectories were followed over time until equilibration, with attention paid to the relative position and orientation of the CH_3OOH with respect to the rest of the ice cluster and the interactions of water molecules with the peroxide. Snapshots extracted from these simulations were used to obtain a set of starting configurations for the subsequent photolysis simulations.

The potential energies for the ground state and first excited singlet state of isolated CH_3OOH versus O—O distance (Fig. 2) were computed by using configuration interaction singles (25). The excited-state potential is repulsive at the relevant geometries, and dissociation after the Franck–Condon photoexcitation of CH_3OOH begins by breaking the O—O bond. This assumption is supported by previous studies (5, 8). When the CH_3O and OH fragments separate to a distance of 2.6 Å, the ground and excited curves coalesce, and we assumed that at this point the system converts to the ground electronic state. Several trial simulations for CH_3OOH on ice showed that dissipation of energy from the fragments into the cluster was negligible at these early stages of the process. Thus, all trajectories were pursued on the ground-state PM3 potential, starting from fragment distances of r(O—O) ≈ 2.6 Å. All of the excess energy was assumed to go into the translational recoil of the OH and CH_3O fragments parallel to the O—O bond; appropriate values of their initial velocities were calculated from conservation of linear momentum and superimposed onto the thermal velocities. The propagation of all trajectories was pursued on the fly with the PM3.

ACKNOWLEDGMENTS. We thank Dr. O. Schrems (Alfred Wegener Institute, Bremerhaven, Germany) for providing preliminary results of experiments on photolysis of CH_3OOH in ice. This work was supported by the National Science Foundation through the Environmental Molecular Sciences Institute (Grant CHE-0431312). Work at the Hebrew University was supported by Israel Science Foundation Grant 114/08.

1. Lee M, Heikes BG, O'Sullivan DW (2000) Hydrogen peroxide and organic hydroperoxide in the troposphere: A review. *Atmos Environ* 34:3475–3494.
2. Gunz DW, Hoffmann MR (1990) Atmospheric chemistry of peroxides: A review. *Atmos Environ A* 24:1601–1633.
3. Jackson AV, Hewitt CN (1999) Atmosphere hydrogen peroxide and organic hydroperoxides: A review. *Crit Rev Environ Sci Technol* 29:175–228.
4. Hasson AS, Paulson SE (2003) An investigation of the relationship between gas-phase and aerosol-borne hydroperoxides in urban air. *J Aerosol Sci* 34:459–468.
5. Watts JD, Francisco JS (2006) Ground and electronically excited states of methyl hydroperoxide: Comparison with hydrogen peroxide. *J Chem Phys* 125:104301.
6. Hellpointner E, Gaeb S (1989) Detection of methyl, hydroxymethyl and hydroxyethyl hydroperoxides in air and precipitation. *Nature* 337:631–634.
7. Hewitt CN, Kok GL (1991) Formation and occurrence of organic hydroperoxides in the troposphere: Laboratory and field observations. *J Atm Chem* 12:181–194.
8. Matthews J, Sinha A, Francisco JS (2005) Unimolecular dissociation and thermochemistry of CH_3OOH. *J Chem Phys* 122:221101.
9. Monod A, et al. (2007) Photooxidation of methylhydroperoxide and ethylhydroperoxide in the aqueous phase under simulated cloud droplet conditions. *Atmos Environ* 41:2412–2426.
10. Ravetta F, et al. (2001) Experimental evidence for the importance of convected methylhydroperoxide as a source of hydrogen oxide (HO_x) radicals in the tropical upper troposphere. *J Geophys Res* 106:32709–32716.
11. Snow JA, et al. (2003) Winter-spring evolution and variability of HO_x reservoir species, hydrogen peroxide, and methyl hydroperoxide, in the northern middle to high latitudes. *J Geophys Res* 108:TOP 10/11–TOP 10/15.
12. Valverde-Canossa J, Wieprecht W, Acker K, Moortgat GK (2005) H_2O_2 and organic peroxide measurements in an orographic cloud: The FEBUKO experiment. *Atmos Environ* 39:4279–4290.
13. Hua W, et al. (2008) Atmospheric hydrogen peroxide and organic hydroperoxides during PRIDE-PRD'06, China: Their concentration, formation mechanism and contribution to secondary aerosols. *Atmos Chem Phys* 8:6755–6773.
14. Friedlander SK, Yeh EK (1998) The submicron atmospheric aerosol as a carrier of reactive chemical species: Case of peroxides. *Appl Occup Environ Hygiene* 13:416–420.
15. Jaegle L, et al. (1997) Observed OH and HO_2 in the upper troposphere suggest a major source from convective injection of peroxides. *Geophys Res Lett* 24:3181–3184.
16. Chevallier E, Jolibois RD, Meunier N, Carlier P, Monod A (2004) "Fenton-like" reactions of methylhydroperoxide and ethylhydroperoxide with Fe^{2+} in liquid aerosols under tropospheric conditions. *Atmos Environ* 38:921–933.
17. Claeys M, et al. (2004) Formation of secondary organic aerosols from isoprene and its gas-phase oxidation products through reaction with hydrogen peroxide. *Atmos Environ* 38:4093–4098.
18. Blitz MA, Heard DE, Pilling MJ (2005) Wavelength-dependent photodissociation of CH_3OOH. *J Photochem Photobiol A* 176:107–113.
19. Roehl CM, Marka Z, Fry JL, Wennberg PO (2007) Near-UV photolysis cross-sections of CH_3OOH and $HOCH_2OOH$ determined via action spectroscopy. *Atmos Chem Phys* 7:713–720.
20. Vaghjiani GL, Ravishankara AR (1990) Photodissociation of hydrogen peroxide and methyl hydroperoxide (CH_3OOH) at 248 nm and 298 K: Quantum yields for hydroxyl, atomic oxygen, and atomic hydrogen ($O(^3P)$, and $H(^2S)$). *J Chem Phys* 92:996–1003.
21. Thelen MA, Felder P, Huber JR (1993) The photofragmentation of methyl hydroperoxide (CH_3OOH) at 193 and 248 nm in a cold molecular beam. *Chem Phys Lett* 213:275–281.
22. Wang C, Chen Z (2006) Effect of CH_3OOH on the atmospheric concentration of OH radicals. *Progr Nat Sci* 16:1141–1149.
23. Novicki SW, Vasudev R (1990) Photodissociation of methyl hydroperoxide at 266 nm: Vector correlations and energy distribution in the hydroxyl fragment. *J Chem Phys* 93:8725–8730.
24. Vione D, et al. (2006) Photochemical reactions in the tropospheric aqueous phase and on particulate matter. *Chem Soc Rev* 35:441–453.
25. Foresman JB, Head-Gordon M, Pople JA, Frisch MJ (1992) Toward a systematic molecular orbital theory for excited states. *J Phys Chem* 96:135–149.
26. Andersson S, Kroes G-J, van Dishoeck EF (2005) Photodissociation of water in crystalline ice: A molecular dynamics study. *Chem Phys Lett* 408:415–421.
27. Woittequand S, et al. (2007) Classical and quantum studies of the photodissociation of a HX (X = Cl, F) molecule adsorbed on ice. *J Chem Phys* 127:164711–164717.
28. Woittequand S, et al. (2007) Photodissociation of a HCl molecule adsorbed on ice at T = 210 K. *Surf Sci* 601:3034–3041.
29. Inglese S, Granucci G, Laino T, Persico M (2005) Photodissociation dynamics of chlorine peroxide adsorbed on ice. *J Phys Chem B* 109:7941–7947.
30. Kosloff R, Zeiri Y (1992) A theoretical study of hydrogen diffraction following photodissociation of adsorbed molecules. *J Chem Phys* 97:1719–1733.
31. Seideman T (1993) Photodissociation of hydrogen bromide adsorbed on lithium fluoride (001): A quantum mechanical model. *J Chem Phys* 99:4766–4774.
32. Cwiklik L, Kubisiak P, Kulig W, Jungwirth P (2008) Reactivity of a sodium atom in vibrationally excited water clusters: An ab initio molecular dynamics study. *Chem Phys Lett* 460:112–115.
33. Gerber RB, Sebek J (2009) Dynamics simulations of atmospherically relevant molecular reactions. *Int Rev Phys Chem* 28:207–222.
34. Stewart JJP (1989) Optimization of parameters for semiempirical methods. I. Method. *J Comput Chem* 10:209–220.
35. Taketsugu T, Gordon MS (1995) Dynamic reaction coordinate analysis: An application to $SiH_4 + H^- \rightarrow SiH_5^-$. *J Phys Chem* 99:8462–8471.
36. Vaghjiani GL, Turnipseed AA, Warren RF, Ravishankara AR (1992) Photodissociation of hydrogen peroxide at 193 and 222 nm: Products and quantum yields. *J Chem Phys* 96: 5878–5886.
37. Yu X-Y, Barker JR (2003) Hydrogen peroxide photolysis in acidic aqueous solutions containing chloride ions. II. Quantum yield of HO(aq) radicals. *J Phys Chem A* 107:1325–1332.

38. Crowell RA, Lian R, Sauer MC, Oulianov DA, Shkrob IA (2004) Geminate recombination of hydroxyl radicals generated in 200-nm photodissociation of aqueous hydrogen peroxide. *Chem Phys Lett* 383:481–485.
39. Chu L, Anastasio C (2005) Formation of hydroxyl radical from the photolysis of frozen hydrogen peroxide. *J Phys Chem A* 109:6264–6271.
40. Monod A, Chebbi A, Durand-Jolibois R, Carlier P (2000) Oxidation of methanol by hydroxyl radicals in aqueous solution under simulated cloud droplet conditions. *Atmos Environ* 34:5283–5294.
41. Curtiss LA, Frurip DJ, Blander M (1979) Studies of molecular association in water and heavy water vapors by measurement of thermal conductivity. *J Chem Phys* 71:2703–2711.
42. Feyereisen MW, Feller D, Dixon DA (1996) Hydrogen bond energy of the water dimer. *J Phys Chem* 100:2993–2997.
43. Goldman N, et al. (2002) Spectroscopic determination of the water dimer intermolecular potential-energy surface. *J Chem Phys* 116:10148–10163.